Chloride Cofactor in the Photosynthetic Oxygen-Evolving Complex Studied by Fourier Transform Infrared Spectroscopy†

Koji Hasegawa,* Yukihiro Kimura, and Taka-aki Ono*

Laboratory for Photo-Biology (I), RIKEN Photodynamics Research Center, The Institute of Physical and Chemical Research, 519-1399 Aoba, Aramaki, Aoba, Sendai 980-0845, Japan

Received August 7, 2002; Revised Manuscript Received September 12, 2002

ABSTRACT: Fourier transform infrared (FTIR) spectroscopy, using midfrequency S_2/S_1 FTIR difference spectra, has been applied to studies of chloride cofactor in the photosynthetic oxygen-evolving complex (OEC) to determine the effects of Cl^- depletion and monovalent anion substitution. Cl^- depletion resulted in the disappearance of a large part of the amide I and II vibrational modes, and induced characteristic modification in the features of the stretching modes of the carboxylate ligands of the Mn cluster. The normal spectral features were largely restored by replenishment of Cl^- except for some changes in amide bands. The overall features of Br^--, I^--, or NO_3^--substituted spectra were similar to those of the Cl^--reconstituted spectrum, consistent with their ability to support oxygen evolution. In contrast, the spectrum was significantly altered by the replacement of Cl^- with F^- or CH_3COO^-, which resulted in marked suppression and distortion of both the carboxylate and amide bands. The activity of oxygen evolution restored by NO_3^- was as high as that by Cl^- when measured under limited light conditions, indicating that the NO_3^--substituted OEC is fully active in oxygen evolution, although with a slow turnover rate. The double-difference spectrum between the $^{14}NO_3^-$-substituted and $^{15}NO_3^-$-substituted S_2/S_1 difference spectrum showed isotopic bands for asymmetric NO stretching mode in the region of 1400−1300 cm^{-1} due to NO_3^- bound to the Cl^- site. This demonstrated structural coupling between the Cl^- site and the Mn cluster. A proposed model for the isotopic bands suggested that Cl^- as well as NO_3^- is not directly associated with the Mn cluster and exists in a more symmetric configuration and weaker binding state in the S_2 state than in the S_1 state. These results also suggest that Cl^- is required for changes in the structure of the specific carboxylate ligand of the Mn cluster as well as the peptide backbone of protein matrixes upon the transition from S_1 to S_2.

Photosynthetic oxygen evolution is carried out by an oxygen-evolving complex (OEC)[1] residing on the donor side of photosystem II, in which a tetranuclear Mn cluster provides a catalytic site for water oxidation. The reaction comprises five intermediate states labeled S_0-S_4, where S_1 is thermally stable in the dark. Upon absorption of a photon by PS II, the S_1 state advances in a stepwise fashion to reach the S_4 state, and then decays to the S_0 state with concurrent release of an oxygen molecule (reviewed in refs *1*−*3*).

Cl^- is an essential inorganic cofactor for the normal function of the OEC. O_2 evolution is inhibited by depletion of Cl^- and is restored by replenishment with Cl^- (*1*−*5*). Isotope labeling studies with PS II membranes from spinach grown with supplementation by $Na^{36}Cl$ have suggested that the membranes have a binding site for approximately one Cl^- ion per unit of PS II, and the Cl^- ion at the site slowly exchanges with that in the bulk medium (*6*, *7*). Retention of the functional Cl^- largely depends on the presence of 16 and 24 kDa extrinsic proteins, which constitute a diffusion barrier for preventing exchange of Cl^- and/or a concentrator for Cl^-. The removal of the proteins leads to a decrease in the apparent affinity of the site for Cl^- as revealed by the requirement of higher concentrations of Cl^- for supporting O_2 evolution, and an increase in the accessibility of the site by external anions (*8*−*12*). It has been shown that the binding affinity for Cl^- depends on the oxidation state of the OEC, for which the affinity is lower in the S_2 state than in the S_1 state (ref *13*, but see ref *14*). Effects of Cl^- depletion on the S state turnover events have been extensively studied with various experimental techniques. In the absence of Cl^-, the S state transition is interrupted after reaching the S_2 state (*15*−*19*), and further illumination induces the state to give a $g = 2$ split-type signal (*20*, *21*). Measurements of flash-induced UV absorption changes in combination with a rapid Cl^- removal technique showed that Cl^- is required for the S_2-to-S_3 and S_3-to-S_0 transitions (*22*). In contrast, it has been suggested that all the PS II centers are able to evolve O_2, although at a much reduced rate, even in the absence of Cl^-

† This work was supported by grants for the Frontier Research System at RIKEN and a Grant-in-Aid for Scientific Research (13640695) (to T.O.) from MECSST of Japan.

* To whom correspondence should be addressed. Telephone: +81-22-228-2047. Fax: +81-22-228-2045. E-mail: kojihase@postman.riken.go.jp or takaaki@postman.riken.go.jp.

[1] Abbreviations: Chl, chlorophyll; DCMU, 3-(3,4-dichlorophenyl)-1,1-dimethylurea; EPR, electron paramagnetic resonance; EXAFS, extended X-ray absorption fine structure; FTIR, Fourier transform infrared; Mes, 2-morpholinoethanesulfonic acid; OEC, oxygen-evolving complex; PPBQ, phenyl-*p*-benzoquinone; PS, photosystem; Q_A, primary quinone acceptor of photosystem II; Q_B, secondary quinone acceptor of photosystem II; TL, thermoluminescence; Y_D, tyrosine 161 of the D2 protein; Y_Z, redox active tyrosine 161 of the D1 protein.

10.1021/bi026595n CCC: $22.00
Published on Web 10/23/2002

in membranes depleted of Cl^- by the dialysis method (*7*). Although the Cl^--depleted S_2 state does not show the S_2 multiline EPR signal, the oxidation of the Mn cluster has been demonstrated by the K-edge shift of the Mn XANES spectrum (*19*).

The Cl^- ion can be functionally replaced with other monovalent anions, which serve oxygen evolution with decreasing effectiveness in the following order: $Cl^- \geq Br^- > NO_3^- > NO_2^- > I^-$ under saturating light intensity (*4*, *11*, *23*−*25*). O_2 evolution activity supported by I^- depends on the concentration of free I^- in the bulk medium, which donates electrons to the OEC in competition with water (*26*). The kinetics of the S_4-to-S_0 transition are selectively influenced by these surrogate anions. The affected transition rate cannot, however, account for the supported oxygen evolution rate, but it is correlated with the instability of the higher S states induced by the anions (*25*). It has been reported that F^--substituted membranes, produced from Cl^--depleted membranes obtained via pH 10 treatment, can evolve O_2 with a reduced rate (*27*). N_3^-, SO_4^{2-}, and CH_3COO^- may be associated with the Cl^--binding site, but these anions do not support O_2 evolution (*4*, *24*, *28*). Anion substitutions induce changes in the magnetic and redox properties of the Mn cluster as revealed by alterations in the appearance of the S_2 state multiline and/or $g = 4$ EPR signals and the generation of the TL bands with variously changed peak temperatures (*11*, *24*, *25*, *27*, *29*−*32*). These anion-dependent property changes of the Mn cluster have been interpreted to mean that Cl^- is bound in the proximity of the Mn cluster. The Mn EXAFS spectrum showed some alterations when cyanobacteria were cultured in a medium supplemented with Br^- as a replacement for Cl^- (*31*), and when the Cl^- site was occupied by F^- (*33*). These suggest that the presence of Cl^- in the vicinity of the Mn cluster and/or the ligation structure of the Mn cluster is affected by the replacement of Cl^- with Br^- or F^-. Simulation of the pulsed EPR spectrum of the split signal induced in acetate-inhibited PS II membranes suggested that acetate is located within approximately 3.5 Å of the Y_Z radical (*32*). This has been interpreted to mean that the Cl^- binding site is in the proximity of Y_Z and the Mn cluster since acetate is thought to replace Cl^- in a competitive manner. A comparison between electron spin-echo envelope modulation spectra of the multiline signals induced in the Br^--substituted and Cl^--reconstituted membranes suggested nuclear coupling between the halide and the Mn cluster in salt-washed membranes, although such coupling was not detected in the membranes where Cl^- was depleted by alkaline pH treatment in the presence of sulfate (*34*). These results may be compatible with the view that Cl^- is bound to the Mn cluster as a direct ligand, but no direct experimental evidence for this has been reported. That Cl^- is a Mn ligand was also suggested by the analyses of the inhibitory effects of primary amines on O_2 evolution in competition with Cl^- (*23*).

Despite these many and extensive studies, the role of Cl^- in the water oxidation reaction still remains largely unresolved. To address this issue, it seems important to elucidate the properties of the Cl^- binding site, the binding mode of Cl^- at the site, and possible structural changes of the protein matrixes that are related to Cl^- and the oxidation of the Mn cluster. Most previously utilized experimental techniques for studies on the Cl^- cofactor in OEC, however, are not adequate for providing information about these subjects directly, although they may be very useful for monitoring possible changes in structural, redox, and magnetic properties of the Mn cluster itself and for kinetic analyses of S state turnover events. FTIR spectroscopy is a powerful tool for investigating detailed structural changes of protein matrixes and small molecules associated with proteins, and has been successfully applied to the studies on many biological enzymes. In recent years, the FTIR technique has been extensively applied to the study of photosynthetic oxygen evolution (*35*−*51*). Light-induced FTIR difference spectroscopy has enabled us to probe subtle conformation and/or configuration changes of protein matrixes of the OEC upon the S state transition, including the ligands of the Mn cluster and water molecules interacting with the OEC (*47*, *48*, *51*). The technique has been also applied to the studies of the functional Ca^{2+} in the OEC, and some interesting and useful information elucidating the role of Ca^{2+} in oxygen evolution has been obtained (*37*, *50*). But, as far as we know, no FTIR study has been conducted on the Cl^- cofactor in the OEC except for one brief and preliminary result given in ref *52*. In the study presented here, we systematically examined the effects of Cl^- depletion and the replacement of Cl^- by other monovalent anions on the S_2/S_1 FTIR difference spectrum in the midfrequency region. To avoid further complexity caused by the 16 and 24 kDa proteins, which might be partially liberated during treatments for Cl^- depletion, thereby inducing apparent heterogeneity in samples, we depleted these two proteins with high-salt treatment, followed by extensive washing with Cl^--free medium for depleting Cl^-. We also report the S_2/S_1 FTIR difference spectrum of NO_3^- that is functionally bound to the Cl^- site, obtained as the isotopic difference spectrum between $^{14}NO_3^-$ and $^{15}NO_3^-$.

MATERIALS AND METHODS

Sample Preparations. BBY-type PS II membranes were prepared from spinach, as has been described previously (*53*), with modifications (*54*), and stored in liquid N_2 until they were used. For Cl^- depletion, the dark-adapted PS II membranes, after two washes with a medium containing 400 mM sucrose, 20 mM NaCl, 20 mM $CaCl_2$, and 20 mM Mes/NaOH (pH 6.5), were suspended in a medium containing 2 M NaCl, 400 mM sucrose, and 20 mM Mes/NaOH (pH 6.5) at 0.5 mg of Chl/mL. The suspension was then incubated at 0 °C for 25 min under complete darkness to facilitate the removal of the 16 and 24 kDa extrinsic proteins. The salt-treated membranes were extensively washed (at least seven times) with a medium containing 400 mM sucrose and 20 mM Mes/NaOH (pH 6.5) supplemented with $^1/_{10}$ volume of a medium containing 100 mM $Ca(OH)_2$ and 300 mM Mes (pH 6.4) (medium A). All chemicals for medium A were from Sigma Ultra except for $Ca(OH)_2$ (99.9%, Wako Pure Chemical Industries). The resulting membranes (Cl^--depleted membranes) were suspended in medium A at 0.5 mg of Chl/mL supplemented with no or the specified anions (40 mM), and then incubated on ice for 1 min. No detectable changes were observed in the FTIR and TL features after a prolonged incubation time (for at least 6 h). Sample membranes included 0.1 mM DCMU for measuring the $S_2Q_A^-/S_1Q_A$ FTIR difference spectrum and TL glow curve for $S_2Q_A^-$ charge recombination, and 0.1 mM DCMU and 10 mM NH_2OH for the Q_A^-/Q_A FTIR difference spectrum (*35*, *37*,

50). NH_2OH was added as a NH_2OH solution (50% stock, Wako Pure Chemical Industries) prepared just before it was used. The pH of medium A was preadjusted to 6.5 after the addition of the NH_2OH solution. NH_2OH and DCMU were added as an exogenous electron donor and as an inhibitor of the electron transfer from Q_A to Q_B, respectively. Sample preparations and the following procedures were performed under complete darkness or dim green light unless otherwise noted. For FTIR, sample suspensions were centrifuged for 30 min at 176000*g*, and the resultant pellet was sandwiched between a pair of BaF_2 plates. $Na^{15}NO_3$ (99.5% ^{15}N enrichment) was purchased from Shoko Tsusho.

Measurements. FTIR spectra were recorded on a Bruker IFS-66V/S spectrophotometer equipped with an MCT detector (EG&G OPTOELECTRONICS model J15D16-M204B-S01M-60-D316/6). A custom-made CdTe band-pass filter ($2000-350\ cm^{-1}$) was placed in front of the sample to eliminate the He−Ne laser scatter from the interferometer compartment, and to improve the signal quality. The sample temperature was controlled at 250 K using a custom-built cryostat and a temperature controller (Chino, KP1000). Samples were illuminated with a continuous-wave (CW) light (HOYA-SCHOTT) passing through a long-pass filter (>620 nm). The light-minus-dark FTIR difference spectrum was obtained by subtracting the single-beam dark spectrum from that following illumination. Each single-beam spectrum was measured at 4 cm^{-1} resolution by averaging 150 scans (65 s accumulation). Four to six spectra for different samples were averaged to improve the signal-to-noise ratio. Analyses of spectra were carried out using the Bruker OPUS program, version 3.03, without data smoothing. The S_2/S_1 difference spectrum was obtained by subtracting the Q_A^-/Q_A difference spectrum from the $S_2Q_A^-/S_1Q_A$ difference spectrum (*37*, *50*). Thermoluminescence was measured using a custom-built apparatus. Samples (0.15 mg of Chl/mL) were illuminated at 250 K with CW light (>620 nm) for 5 s, followed by rapid cooling in liquid N_2. The light emission during sample warming was recorded versus sample temperature. O_2 evolving activity was measured at 25 °C using a Clark-type O_2 electrode in medium A supplemented with the specified anions in the presence of 0.25 mM PPBQ. Light intensity was changed with appropriate neutral density filters.

Determination of the Cl^- Concentration. The concentrations of free Cl^- in solutions were determined photometrically by the reaction of Cl^- with mercuric thiocyanate in the presence of ferric iron to form mercuric chloride, chloromercurate(II) anions, and ferric thiocyanate using Chloride Test (Merck).

RESULTS

Figure 1 shows the concentration dependence of various anions on the restoration of the O_2 evolution in the Cl^--depleted membranes used for FTIR measurements under saturating light (panel A) and limiting light (panel B) conditions. As shown in panel A, the O_2 evolution was suppressed in the Cl^--free medium (<30 μM Cl^-) almost completely, and the O_2 evolution was pronouncedly restored by Cl^- addition. Nearly 90% of the untreated control activity was restored at 20 mM Cl^- (see Table 1) and remained constant up to 100 mM Cl^-. More than 80% of the saturation level activity was restored at 5 mM Cl^-. Br^- restored the

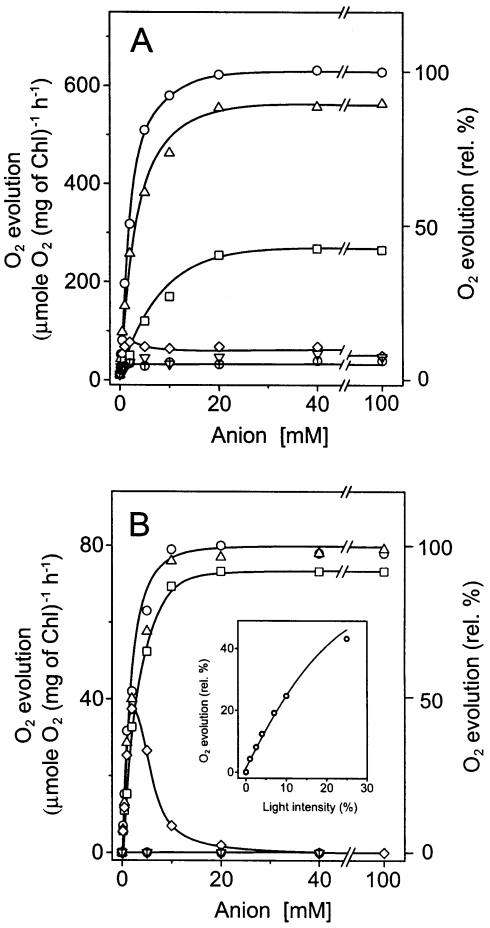

FIGURE 1: Dependence of O_2 evolution on anion concentration in Cl^--depleted PS II membranes under saturating light (A) and limiting light (B) conditions. The extent of O_2 evolution was measured in the presence of various concentrations of Cl^- (○), Br^- (△), NO_3^- (□), I^- (◇), F^- (▽), and CH_3COO^- (Φ). O_2 evolution was assessed at 5 and 25 μg of Chl/mL for saturating and limiting light conditions, respectively. The inset shows the light intensity dependence of O_2 evolution in the presence of 40 mM Cl^-. See the text for other details.

O_2 evolution in a manner similar to that of Cl^-, although the maximum activity restored by Br^- was somewhat lower than that restored by Cl^-. The O_2 evolution restored by NO_3^- was less than 40% of that by Cl^-, and the concentration of NO_3^- required for the restoration was higher than that of Cl^- or Br^-. The apparent K_m values of Cl^-, Br^-, and NO_3^- for the restoration of O_2 evolution were found to be 2, 3, and 7 mM, respectively. I^- restored the O_2 evolution to some extent at lower concentrations (<2 mM), but the restoration tended to be suppressed at higher concentrations. F^- and CH_3COO^- showed little restoration of O_2 evolution except for a very faint increment of the activity.

Cl^--dependent restoration of the O_2 evolution was also assessed at a limited light intensity as shown in panel B, in which the light intensity was reduced to 4% of the saturated light intensity and the sample concentration was increased by 5-fold for measuring the lower activity more precisely. The light limitation was confirmed by the linearity of the activity with respect to the light intensity as shown in the inset, and by no activity change when the concentration of PPBQ was doubled. Under these conditions, the level of O_2 evolution was negligibly small in the absence of Cl^- and markedly restored by the addition of Cl^-. Although the

Table 1: Effects of Cl^- Depletion and Anion Substitutions on O_2 Evolution, Apparent K_m Values, and Thermoluminescence ($S_2Q_A^-$) Bands

sample membrane	O_2 evolution [μmol of O_2 (mg of Chl)$^{-1}$ h^{-1}]	apparent K_m (mM)	$S_2Q_A^-$ thermoluminescence band: peak temperature (°C)	$S_2Q_A^-$ thermoluminescence band: relative intensity (%)[a]
control	718 (100)[b]		12	100
Cl^--depleted				
no addition	13 (2)	ND[c]	31	97
with F^-[d]	53 (7)	—[e]	24	104
with Cl^-	632 (88)	2	11	98
with Br^-	557 (78)	3	17	101
with I^-	67 (9)	—[e]	—[f] (25)[g]	0 (24)[g]
with NO_3^-	268 (37)	7	24	97
with CH_3COO^-	39 (5)	—[e]	30	105

[a] The intensity was estimated from integration of the area under the thermoluminescence glow curve. [b] Numbers in parentheses represent the oxygen-evolving activity in relative percent. [c] No data. [d] Anion (40 mM) was added as sodium salt. [e] No reliable K_m was obtained. [f] No thermoluminescence band was induced. [g] Data of sample membranes reconstituted with 5 mM I^-.

restored activity at the saturated Cl^- concentration was as low as approximately 10% of that under saturating light conditions, the normalized Cl^- dependence curves obtained under saturating and limiting light conditions are very similar. This strongly indicates that the OEC is inactivated in an all-or-none manner in the Cl^--depleted membranes used in this study. Br^- showed a dependence curve quite similar to that of Cl^- with the same saturation level of O_2 evolving activity. In contrast to the saturating light conditions, the O_2 evolution restored by NO_3^- was comparable to the activity by Cl^-, indicating that the NO_3^--substituted OEC is fully active in O_2 evolution but has a slower turnover rate. The apparent K_m of NO_3^- was somehow smaller under the limiting light than under the saturating light conditions. This seems to be related to the fact that the kinetically obtained apparent K_m is not a true dissociation constant and may reflect another reaction process, but the exact reason for the difference is not sufficiently clear at present. The O_2 evolution restored by I^- was largely comparable to that restored by Cl^- at lower I^- concentrations (<2 mM), and the maximum activity was approximately 50% of the activity restored by Cl^-. Then, the activity decreased with increasing I^- concentration to be negligibly small above 20 mM. The observed effects of I^- on O_2 evolution are consistent with the report that I^- supports a relatively high level of O_2 evolution in the Cl^--depleted preparation reconstituted with the extrinsic 16 and 24 kDa proteins when the concentration in a bulk medium is kept low (*26*), and the view that a high concentration of I^- in a bulk medium donates an electron to the donor side of PS II to interrupt oxidation of the Mn cluster (*26*, *55*). The much higher recovery of O_2 evolution under the limiting as opposed to the saturating light conditions indicates that the turnover rate of the O_2-evolving reaction in the I^--substituted OEC is retarded compared with that of the Cl^--reconstituted control OEC.

Table 1 shows the effects of Cl^- depletion and anion (40 mM) substitution on O_2 evolution, and the apparent K_m for the restoration of the O_2 evolution under saturating light conditions. The O_2 evolution activity was markedly suppressed by Cl^- depletion but largely restored by replenishment of Cl^- and Br^-. Approximately 40% activity was restored by NO_3^-, but little activity restoration was observed with I^-, F^-, or CH_3COO^-. The effects of anion substitution on O_2 activity are consistent with those reported in thylakoid and PS II membranes which were depleted of Cl^- by various different procedures (*11*, *18*, *24*, *25*, *56*, *57*). Table 1 also shows the peak temperature and intensity of the thermoluminescence (TL) band arising from the $S_2Q_A^-$ state which was induced by illuminating the membranes under conditions identical to those for the FTIR measurements. The peak temperature of the $S_2Q_A^-$ band found at 12 °C in the control membranes was upshifted to 31 °C by Cl^- depletion. The Cl^- reconstitution restored an almost normal peak temperature, which was upshifted to 17 °C by Br^- substitution, further to 24 °C by F^- and NO_3^- substitution, and to 30 °C by CH_3COO^- substitution. The results indicate that the redox property of the S_2 state Mn cluster is changed depending on the substituting anions. Despite these changes, the yield of the S_2 state induced in the anion-substituted membranes was comparable to that of the Cl^--reconstituted membranes. No TL band was induced in the membranes substituted with 40 mM I^-, consistent with little restoration of O_2 evolution, and this may be ascribed to the reduction of the S_2 state Mn cluster by bulk I^-. Indeed, a TL band was developed at 25 °C in the membranes substituted with 5 mM I^-, although the band intensity was considerably low. The peak temperatures of these anion-substituted bands were higher than those of the control and Cl^--reconstituted bands, but no linear relationship appeared between the TL peak temperature and the O_2 evolving activity. The effects of anion substitution on $S_2Q_A^-$ TL peak temperature in this study are substantially compatible with those for the $S_2Q_B^-$ TL band (*24*), despite differences in some details. These differences are probably caused by the difference in the procedure for Cl^- depletion and anion substitution, which were performed at pH 7.5 without pretreatment for the depletion of the 16 and 24 kDa extrinsic proteins. It has been proposed that NO_3^- enhances the decay of the higher S states presumably by reducing the Mn cluster (*13*). However, the TL data indicate that the S_2 state is stably formed with high efficiency in the NO_3^--substituted OEC as compared with those of the Cl^--reconstituted and untreated control OECs. This view is also consistent with the result that the O_2 evolution restored by NO_3^- is comparable to that restored by Cl^- under the limiting light conditions as shown in Figure 1. The faster decay of the higher S states found in ref *13* may be explained by assuming the reduction of the higher S state Mn cluster in the NO_3^--substituted OEC by the redox reagents which were included in the reaction mixture and reduced during illumination.

Figure 2 shows the effects of Cl^- depletion on the S_2/S_1 FTIR difference spectrum. The S_2/S_1 spectrum was obtained by subtracting the Q_A^-/Q_A difference spectrum from the $S_2Q_A^-/S_1Q_A$ difference spectrum after normalizing both spectra with respect to the intensity of the CO stretching band of Q_A^- at 1479 cm^{-1} (refs *35*, *36*, *41*, *45*, *50*, *58*, and *59*, but see ref *60*). The characteristic vibrational features of the S_2/S_1 difference spectrum in untreated control PS II membranes (spectrum a) (*35*−*41*, *43*−*46*, *48*, *50*) are markedly changed by Cl^- depletion (spectrum b): the differential bands in the amide I (1690−1630 cm^{-1}) and amide II (1590−1515 cm^{-1}) regions were largely suppressed

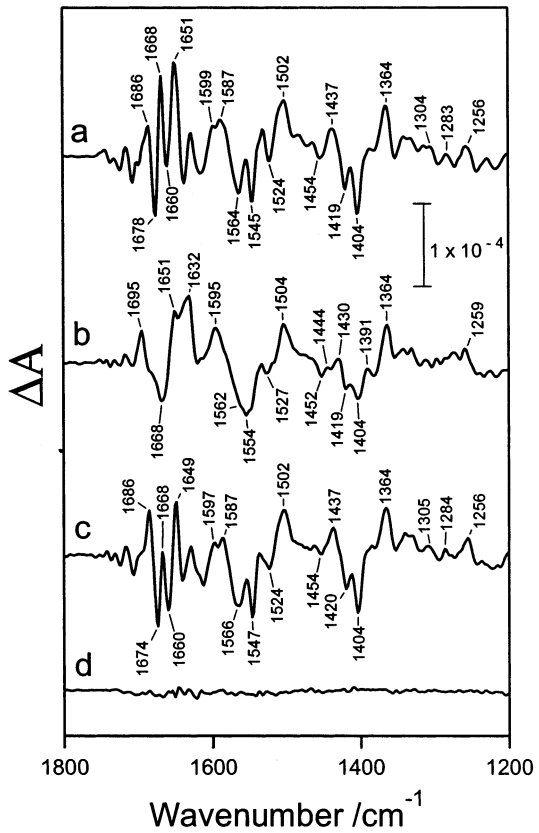

FIGURE 2: Light-induced S_2/S_1 FTIR difference spectra of (a) untreated control, (b) Cl^--depleted, and (c) Cl^--reconstituted (with 40 mM NaCl) PS II membranes. Each S_2/S_1 difference spectrum was obtained by subtracting the Q_A^-/Q_A difference spectrum from the $S_2Q_A^-/S_1Q_A$ difference spectrum (see the text for details). A dark-minus-dark FTIR spectrum (d) is presented to show the noise level. Sample membranes were illuminated with continuous light (2 mW/cm^2) at 250 K for 10 s. The sample suspension included 0.1 mM DCMU for the $S_2Q_A^-/S_1Q_A$ difference spectrum or 0.1 mM DCMU and 10 mM NH_2OH for the Q_A^-/Q_A difference spectrum. Spectra were recorded at a resolution of 4 cm^{-1}.

or completely disappeared, and replaced with a broad band at ~1632(+) cm^{-1} and bands at 1668(−) and 1695(+) cm^{-1}. In addition to these major changes, Cl^- depletion suppressed the negative band at 1524 cm^{-1}. Although the CC stretching mode of the phenol ring of the Y_Z tyrosine has been reported to show a band at 1524 cm^{-1} (ref *39*, but see refs *61* and *62*), it is equivocal that the observed band change is ascribed to Y_Z since many other bands can overlap in this region. In addition, the band at 1437(+) cm^{-1} and several bands in the region of 1304−1260 cm^{-1}, the origins of which have not been identified, were also suppressed. In contrast, the bands at 1595(+)/1562(−) cm^{-1} for asymmetric and at 1364(+)/1404(−) cm^{-1} for symmetric stretching modes of the putative carboxylate ligand for the Mn cluster (*37*, *63*) were still prominent in the Cl^--depleted spectrum. Cl^- depletion did not influence the bands in the 1750−1700 cm^{-1} region that are due to carbonyl stretching modes for protonated acidic amino acid residues (*37*). Notably, no change in the Q_A^-/Q_A vibrational features was induced by Cl^- depletion (data not shown), indicating that Cl^- depletion does not affect Q_A and its proximal protein environment. The 1695(+), 1632(+), and 1504(+) cm^{-1} bands found in the Cl^--depleted spectrum coincide with some bands in the Y_D^+/Y_D difference spectrum (*39*, *58*), and therefore, these bands may be attributable to partial oxidation of Y_D tyrosine in the Cl^--depleted membranes. This view is, however, not compatible with the observation that other intense and characteristic bands for the Y_D^+/Y_D vibrational features were not revealed in the Cl^--depleted spectrum. Furthermore, some of those bands were also prominent in the untreated control S_2/S_1 spectrum. The characteristic S_2/S_1 vibrational structure, which disappeared with Cl^- depletion, was largely restored by the subsequent reconstitution of Cl^- (spectrum c), consistent with significant restoration of the O_2 evolving activity (see Table 1). There is, however, a difference in the amide I region between the untreated control and Cl^--reconstituted spectrum: the band at 1668(+) cm^{-1} was less pronounced than the other amide bands in the Cl^--reconstituted spectrum. Since nearly 90% O_2 evolution was restored in the Cl^--reconstituted membranes as compared with the untreated control activity, it is unlikely that these changes in the spectrum are attributable to the OEC inactivated during the sample treatments. These two membrane samples differ with respect to the presence (spectrum a) and absence (spectrum c) of the 16 and 24 kDa proteins, but these proteins do not seem to be responsible for the difference in the amide I vibrational features since subsequent reconstitution of these two proteins did not restore the original amide I bands (data not shown). Presumably, the high-NaCl treatment induces some irreversible changes in the OEC protein structure, which are not crucial for O_2 evolution. Consistent with this view, the features of the amide bands of the highly active core preparations from cyanobacteria are markedly different from those of spinach (*39*, *40*, *42*).

Figure 3 shows the effects of Cl^- concentration on the S_2/S_1 FTIR difference spectrum in the Cl^--depleted membranes. It is clearly seen that the spectra changed in their dependence on Cl^- concentration. The features of the spectra in the presence of 0.1 mM Cl^- resembled those of the Cl^--depleted one. In the presence of 0.5 mM Cl^-, the intensity of bands characteristic of the Cl^--depleted spectrum (the bands at 1632 and 1695 cm^{-1}) became low concomitant with the partial development of the bands for the normal spectrum (the bands at 1404, 1668, and 1686 cm^{-1}). The spectrum was rather similar to the Cl^--sufficient spectrum, in the presence of 2 mM Cl^- which corresponds to the apparent K_m for the restoration of O_2 evolution, although the recovery of the spectrum had not yet been accomplished. The spectrum reconstituted with 10 mM Cl^- was almost identical to that reconstituted with 40 mM Cl^- (data not shown). The Cl^- concentration dependence of the restoration of the normal S_2/S_1 FTIR spectrum, although the quantitative representation is difficult due to the complexity of the difference spectrum, was roughly compatible with that of the restoration of O_2 evolution. This suggests that the Cl^- responsible for O_2 evolution participates in the formation changes of the protein matrixes detected by FTIR. We may note, however, in this context that the Cl^- dependence of the recovery of the O_2 evolution does not necessarily coincide with that of the FTIR spectrum, since the former corresponds to the Cl^- dependence of the rate-limiting step of the overall reaction of O_2 evolution while the latter reflects the binding of Cl^- at the S_2 and S_1 states.

The carboxylate bands were prominent in the Cl^--depleted S_2/S_1 difference spectrum. The band intensity of the symmetric stretching vibration, measured peak [1364(+) cm^{-1}]

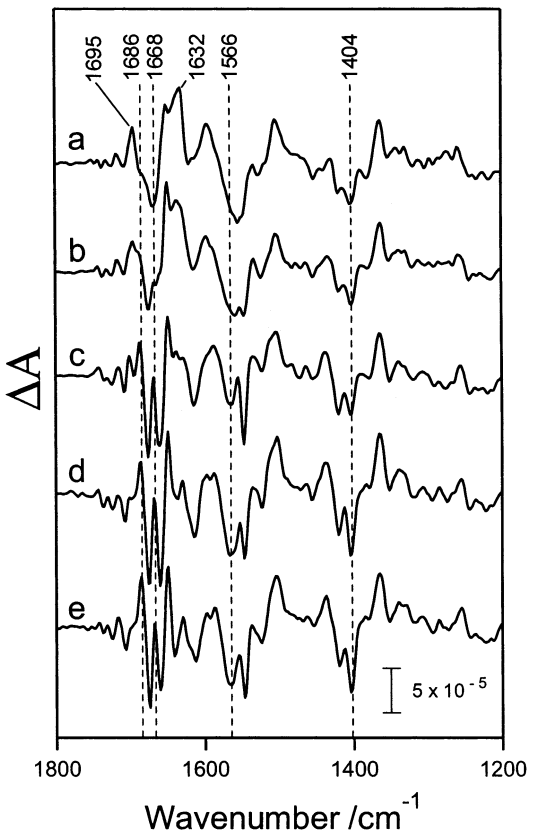

FIGURE 3: Effects of Cl^- concentration on light-induced S_2/S_1 FTIR difference spectra in Cl^--depleted PS II membranes. Sample membranes were illuminated with continuous light (2 mW/cm^2) at 250 K for 10 s in the presence of (a) 0, (b) 0.1, (c) 0.5, (d) 2, and (e) 40 mM Cl^-. Each S_2/S_1 difference spectrum was obtained by subtracting the Q_A^-/Q_A difference spectrum from the $S_2Q_A^-/S_1Q_A$ difference spectrum. See the legend of Figure 2 for other details.

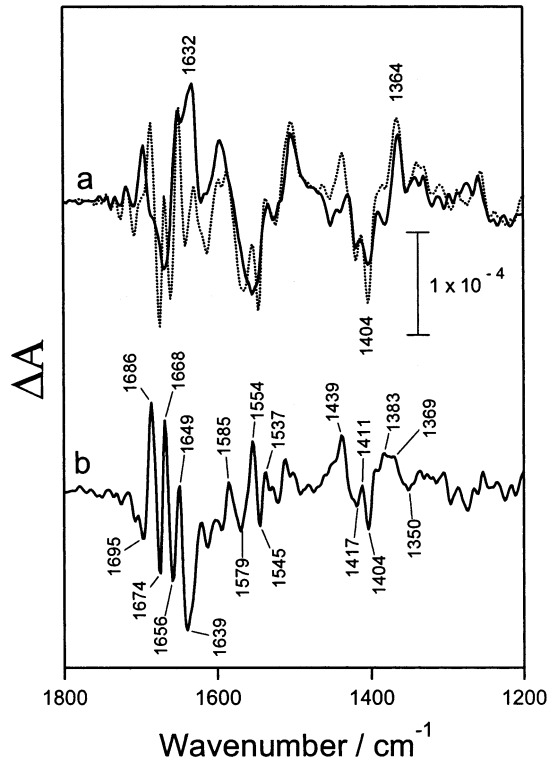

FIGURE 4: Effects of Cl^- depletion on light-induced S_2/S_1 FTIR difference spectra of PS II membranes. (a) Light-induced S_2/S_1 difference spectra of Cl^--depleted (—) and Cl^--reconstituted (with 40 mM NaCl) membranes (•••). (b) Double-difference spectrum obtained by subtracting the Cl^--depleted spectrum (solid curve in part a) from the Cl^--reconstituted spectrum (dotted curve in part a). See the legend of Figure 2 for other details.

to peak [1404(−) cm^{-1}], of the Cl^--depleted S_2/S_1 spectrum was approximately 70% of that of the untreated control S_2/S_1 spectrum. However, close inspection revealed that the vibrational features in the symmetric carboxylate regions were considerably changed by Cl^- depletion. The changes can be observed more clearly in the double-difference spectrum shown in Figure 4, in which the Cl^--depleted S_2/S_1 difference spectrum (a, solid curve) was subtracted from the Cl^--reconstituted S_2/S_1 difference spectrum (a, dotted curve). The resulting double-difference spectrum (b) exhibited negative bands at 1417, 1404, and 1350 cm^{-1} and positive bands at 1439, 1411, and 1383 (1369) cm^{-1}, while the strong positive band at 1364 cm^{-1}, prominent in the Cl^--reconstituted spectrum, was almost completely absent. These results suggest that at least two carboxylate vibrational modes overlap in the carboxylate symmetric stretching region in the control S_2/S_1 difference spectrum, and Cl^- is required for the appearance of one of the two carboxylate modes. Many bands were observed in the amide regions in the double-difference spectrum, indicating that conformational changes in the protein upon S_2 state formation are largely suppressed in the absence of Cl^-. These bands may interfere with the detection of the asymmetric carboxylate mode corresponding to the putative symmetric carboxylate mode in the double-difference spectrum.

Figure 5 shows the S_2/S_1 FTIR difference spectra of anion-substituted PS II membranes. The Cl^--depleted membranes were supplemented with 40 mM monovalent anion, which induces characteristic properties in anion-substituted OECs as shown in Table 1. The S_2/S_1 difference spectrum of the Br^--substituted membranes (spectrum b) was very similar to that of the Cl^--reconstituted membranes (spectrum a), consistent with its high capacity for supporting O_2 evolution (see Table 1 and Figure 1), although the band at 1668(+) cm^{-1} was relatively small and amide II bands were less pronounced in the Br^--substituted S_2/S_1 spectrum. The overall spectral features of the I^--substituted (spectrum c) and NO_3^--substituted (spectrum d) membranes greatly resembled those of the Br^--substituted membranes. At first glance, the appearance of the normal-like spectrum of the I^--substituted membranes seems to be inconsistent with a failure in TL band formation and little recovery of the O_2 evolution in the presence of 40 mM I^-. However, the results can be rationally explained by the interference of electron donation from the bulk I^- to the S_2 state Mn cluster at 250 K, the temperature where FTIR spectra were recorded. The similarities of the FTIR spectra are compatible with Br^-, I^-, or NO_3^- being functionally substituted for Cl^- and showing a high capacity for supporting O_2 evolution as shown in Figure 1. In the NO_3^--substituted S_2/S_1 spectrum, the band at 1524 cm^{-1}, as well as amide II bands, was not distinctively observable. This may be attributable to NO_3^- bound to the Mn cluster as a replacement for Cl^-, since NO stretching modes of the metal binding form of NO_3^- can appear and be superimposed on the amide II and the Y_Z band in this region. However, this is clearly not the case, as shown later in Figure 6. The band at 1524 cm^{-1} was most likely influenced by anion substitution, and slightly shifted to a

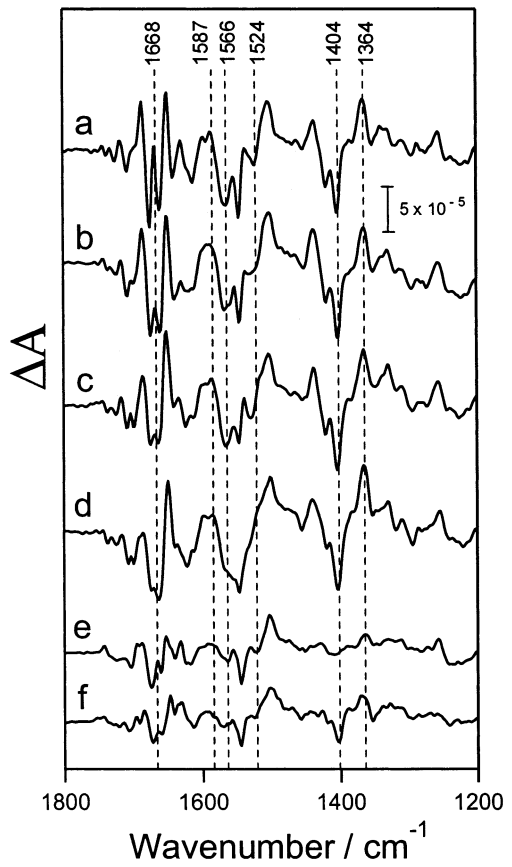

FIGURE 5: Light-induced S_2/S_1 FTIR difference spectra of Cl^--depleted PS II membranes that are reconstituted with (a) Cl^-, (b) Br^-, (c) I^-, (d) NO_3^-, (e) F^-, and (f) CH_3COO^-. For reconstitution, sample membranes were supplemented with 40 mM Na salt of each anion. The S_2/S_1 difference spectrum was obtained by subtracting the Q_A^-/Q_A difference spectrum from the $S_2Q_A^-/S_1Q_A$ difference spectrum. See the legend of Figure 2 for other details.

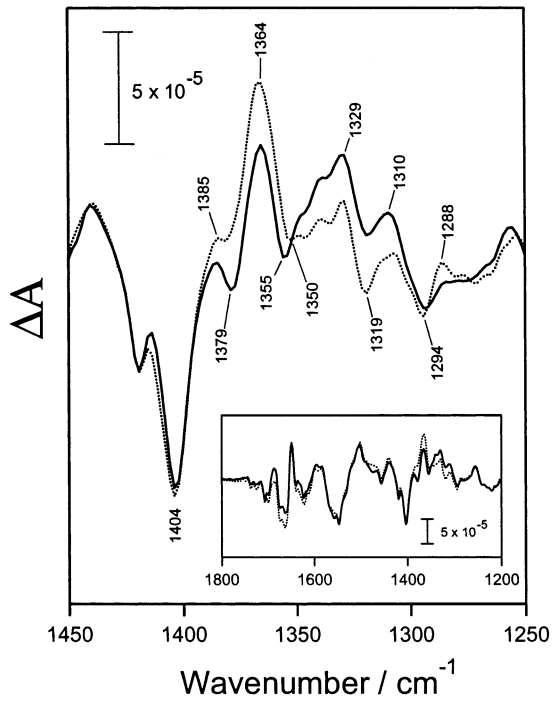

FIGURE 6: Light-induced S_2/S_1 FTIR difference spectra (1450−1250 cm^{-1}) of Cl^--depleted PS II membranes that are reconstituted with 40 mM $Na^{14}NO_3$ (···) or 40 mM $Na^{15}NO_3$ (—). The inset shows the light-induced S_2/S_1 FTIR difference spectra of the mid-IR region (1800−1200 cm^{-1}). Each S_2/S_1 difference spectrum was obtained by subtracting the Q_A^-/Q_A difference spectrum from the $S_2Q_A^-/S_1Q_A$ difference spectrum (see the text for details). Sample membranes were illuminated with continuous light (2 mW/cm^2) at 250 K for 10 s. The sample suspension included 0.1 mM DCMU for the $S_2Q_A^-/S_1Q_A$ difference spectrum or 0.1 and 10 mM NH_2-OH for the Q_A^-/Q_A difference spectrum. Spectra were recorded at a resolution of 4 cm^{-1}.

higher frequency in the I^--substituted S_2/S_1 spectrum. It may therefore be presumed that the overlap of a further upshifted 1524 cm^{-1} band and amide II bands obscures these bands in the NO_3^--substituted S_2/S_1 spectrum. The spectral features of the F^--substituted (spectrum e) and CH_3COO^--substituted (spectrum f) membranes markedly differed from those of the surrogate anions Br^-, I^-, and NO_3^-. The carboxylate stretching bands disappeared (F^- substitution) or were largely suppressed (CH_3COO^- substitution), concomitant with a considerable reduction in the intensities of the bands in the amide I and II regions. It is notable that an identical Q_A^-/Q_A difference spectrum was developed in all anion-substituted membranes (data not shown), indicating that anion substitution and Cl^- depletion do not affect Q_A and its proximal protein environment.

As shown in Table 1 and Figures 1 and 5, NO_3^- can be functionally substituted for Cl^-, indicating that NO_3^- is bound to the Cl^- site in a manner similar to that of Cl^-. NO stretching modes of NO_3^- in various nitrato complexes have been extensively studied, and it has been found that the vibrational modes are very sensitive to the molecular geometry of NO_3^- (*64*−*75*). The NO stretching mode of NO_3^- can, therefore, be used as a potent probe to elucidate the properties of binding of Cl^- to its site and the nature of the binding site. Figure 6 shows the S_2/S_1 FTIR difference spectra of $^{14}NO_3^-$-substituted (dotted curve) and $^{15}NO_3^-$-substituted (solid curve) membranes. The two spectra were almost identical above 1400 cm^{-1} and below 1250 cm^{-1} as shown in the inset, but a distinct difference was observed in the region between 1400 and 1270 cm^{-1}. The ratio of the relative intensities between the 1364(+) and 1329(+) cm^{-1} bands was considerably larger in the S_2/S_1 spectrum of $^{14}NO_3^-$-substituted membranes than in that of $^{15}NO_3^-$-substituted membranes, and the 1379(−) and 1355(−) cm^{-1} bands in the $^{15}NO_3^-$ spectrum became vague in the $^{14}NO_3^-$ spectrum. We note in this context that no isotopic difference was detected in the 1580−1500 cm^{-1} region, where the NO stretching modes of the metal-binding NO_3^- are present. It can therefore be concluded that the apparent changes of the bands in the amide II region in the NO_3^- substitution S_2/S_1 spectrum shown in Figure 5 are not caused by overlapping by the NO modes of NO_3^-.

Figure 7 shows the $^{14}NO_3^-/^{15}NO_3^-$ FTIR difference spectra for the S_2/S_1 (spectrum a), $S_2Q_A^-/S_1Q_A$ (spectra b and d), and Q_A^-/Q_A (spectrum c) difference. The $^{14}NO_3^-$ $(S_2/S_1)/^{15}NO_3^-(S_2/S_1)$ difference spectrum was obtained by subtracting the $^{15}NO_3^-$-substituted S_2/S_1 spectrum from the $^{14}NO_3^-$-substituted S_2/S_1 spectrum, where each S_2/S_1 spectrum was obtained by subtracting the Q_A^-/Q_A difference spectrum from the $S_2Q_A^-/S_1Q_A$ difference spectrum for the $^{14}NO_3^-$-substituted or $^{15}NO_3^-$-substituted membranes. The $^{14}NO_3^-$ $(S_2/S_1)/^{15}NO_3^-$ (S_2/S_1) difference spectrum (spectrum a) exhibited a prominent positive band at approximately 1369 cm^{-1} and a negative band at approximately 1323 cm^{-1}, with minor positive and negative bands at approximately 1288

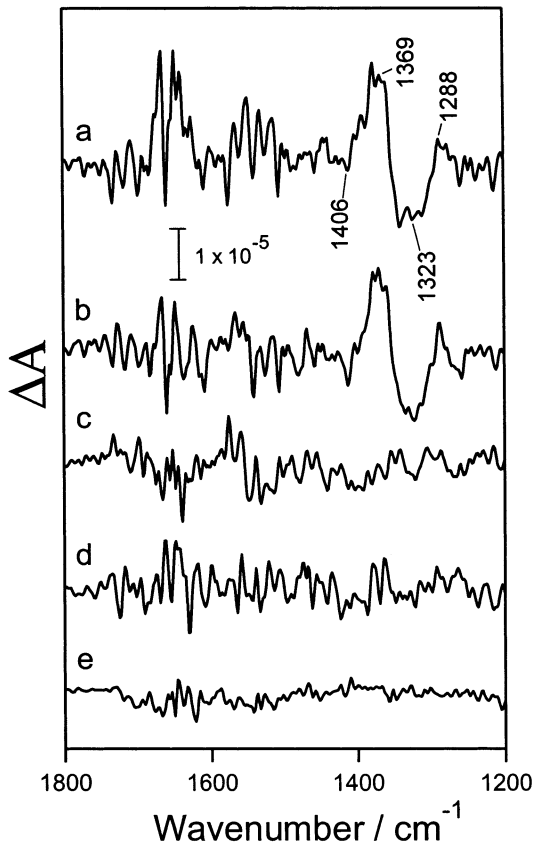

FIGURE 7: $^{14}NO_3^-/^{15}NO_3^-$ FTIR difference spectra for (a) the light-induced S_2/S_1 FTIR difference spectrum, (b and d) the light-induced $S_2Q_A^-/S_1Q_A$ FTIR difference spectrum, and (c) the light-induced Q_A^-/Q_A difference spectrum. The $^{14}NO_3^-/^{15}NO_3^-$ spectrum for the Q_A^-/Q_A difference was obtained by subtracting the $^{15}NO_3^-$-substituted Q_A^-/Q_A spectrum from the $^{14}NO_3^-$-substituted Q_A^-/Q_A spectrum. The $^{14}NO_3^-/^{15}NO_3^-$ spectrum for the $S_2Q_A^-/S_1Q_A$ difference was obtained by subtracting the $^{15}NO_3^-$-substituted $S_2Q_A^-/S_1Q_A$ spectrum from the $^{14}NO_3^-$-substituted $S_2Q_A^-/S_1Q_A$ spectrum. The $^{14}NO_3^-/^{15}NO_3^-$ spectrum for the S_2/S_1 difference was obtained by subtracting the $^{14}NO_3^-/^{15}NO_3^-$ spectrum for Q_A^-/Q_A (spectrum c) from the $^{14}NO_3^-/^{15}NO_3^-$ spectrum for $S_2Q_A^-/S_1Q_A$ (spectrum b). For spectrum d, 20 mM NaCl was further included in the sample suspension. A dark-minus-dark FTIR spectrum (e) was presented to show the noise level. Spectra were recorded at a resolution of 4 cm^{-1}. Five spectra were averaged (750 scans). See the legends of Figures 2 and 6 for other details.

and 1406 cm^{-1}, respectively. On the basis of their peak position, these bands can be ascribed to the asymmetric NO stretching vibrational mode of an ionic NO_3^- (*67*, *68*, *71*−*75*). An identical $^{14}NO_3^-/^{15}NO_3^-$ difference spectrum was obtained for the $S_2Q_A^-/S_1Q_A$ difference (spectrum b) with a better signal-to-noise ratio. No distinct isotopic band, except for these bands, was observed in the spectrum. However, our data cannot completely exclude the possibility that small $^{14}NO_3^-/^{15}NO_3^-$ isotopic bands are concealed behind noise in the region above 1500 cm^{-1}, due to the presence of large water and amide bands. The 1323(−) cm^{-1} band is considerably broader and less intense than the 1369(+) cm^{-1} band, suggesting that the vibrational features of the $^{14}NO_3^-/^{15}NO_3^-$ spectrum are somewhat different between the S_1 and S_2 states. No $^{14}NO_3^-/^{15}NO_3^-$ isotopic band was observed in the Q_A^-/Q_A difference spectrum (spectrum c), indicating that the acceptor side of PS II does not contribute to the isotopic bands found in the S_2/S_1 and $S_2Q_A^-/S_1Q_A$ difference. The isotopic bands were not induced in the $S_2Q_A^-/S_1Q_A$ spectrum

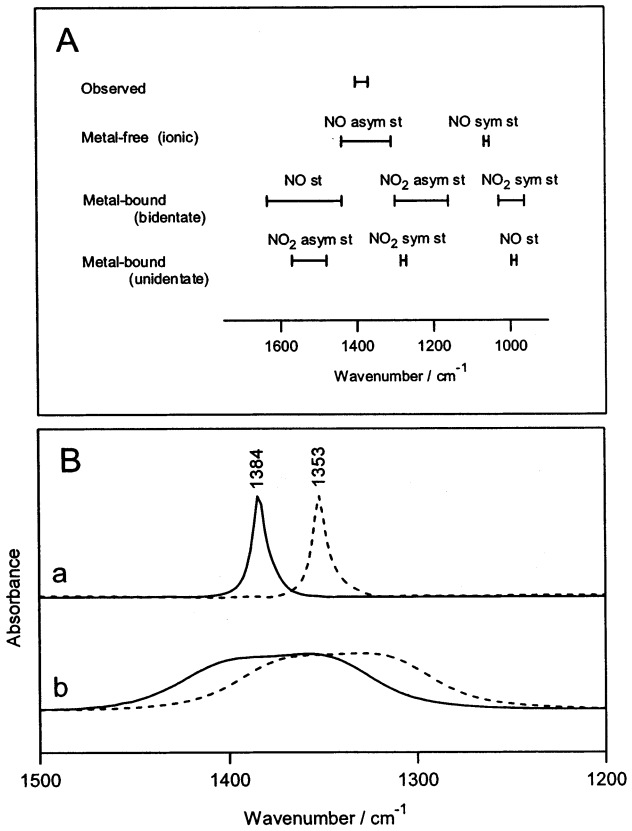

FIGURE 8: (A) Schematic illustration of the frequency region for vibrational stretching modes of NO_3^-. Peak positions of NO_2 and NO stretching modes in the literature (*64*−*75*) are shown for metal-free NO_3^- and NO_3^- bound to transition metals. $^{14}NO_3^-$ bound to the Cl^- site was found to exhibit the bands in the 1400−1370 cm^{-1} region. Abbreviations for vibrational modes: st, stretching; asym, asymmetric; sym, symmetric. (B) IR spectra of the (a) crystal and (b) solution of $Na^{14}NO_3$ (—) and $Na^{15}NO_3$ (···). Spectra were recorded at room temperature.

(spectrum d) when the sample membranes were further supplemented with 20 mM NaCl, which restored the normal O_2 evolution and TL properties in the presence of 40 mM $NaNO_3$ (ref *24* and unpublished results). This strongly indicates that NO_3^- bound to the Cl^- binding site is responsible for the observed $^{14}NO_3^-/^{15}NO_3^-$ isotopic bands.

Figure 8 shows the FTIR spectra of the crystal and solution of $Na^{14}NO_3$ and $Na^{15}NO_3$ (panel B), and the summary of the frequency region for NO_3^- vibrational modes in the literature (*64*−*75*) (panel A). In the crystal, a sharp asymmetric NO stretching band that appeared at 1384 cm^{-1} in $Na^{14}NO_3$ was downshifted by 31 cm^{-1} in $Na^{15}NO_3$, consistent with the reported result (*67*, *71*). The very sharp band in the crystal indicates that a nitrate ion adopts a unique conformation. In contrast, the band was significantly broad in solution, since interactions with water molecules cause variously changed combinations of NO bond length in NO_3^- (*68*, *75*). It is of note, however, that the band of the $Na^{15}NO_3$ solution was downshifted by 31 cm^{-1} as compared with that of the $Na^{14}NO_3$ solution.

DISCUSSION

Vibrational Mode of NO_3^- at the Cl^--Binding Site. This study has demonstrated that the NO stretching vibrational mode of NO_3^- is affected by the oxidation of the Mn cluster upon the S_1 to S_2 transition in NO_3^--substituted membranes,

indicating that Mn oxidation leads to a change in the protein structure of the binding site for NO_3^- for modifying the interaction of an NO_3^- ion with its ligands. Since NO_3^- is functionally substituted for Cl^- (refs *13*, *24*, *25*, *54*, *56*, and *57* and this study) and restored the characteristic S_2/S_1 vibrational features in the Cl^--reconstituted membranes, as shown in Figure 5, it is rational to assume that NO_3^- is functionally bound to the Cl^- binding site. This view is also supported by the disappearance of the isotopic bands on further supplementation of Cl^-, which expels NO_3^- from the Cl^- site. Therefore, these results show that the Cl^- site structurally couples with the Mn cluster, and indicate that the Mn oxidation affects the binding site structure to modulate Cl^- binding. The results are also consistent with the proposal that the Cl^- site is located in the vicinity of the Mn cluster, based on the analyses of Mn EXAFS in the F^-- or Br^--substituted OEC (*31*, *33*), and multiline ESEEM in the Br^--substituted OEC (*34*).

Vibrational spectra of a number of nitrato complexes have been extensively investigated (*64*−*75*). The NO stretching modes of NO_3^- have appeared at 1570−1480 cm^{-1} (NO_2 asymmetric stretching), 1286−1271 cm^{-1} (NO_2 symmetric stretching), and 997−983 cm^{-1} (NO stretching) in unidentate transition metal complexes, and at 1635−1440 cm^{-1} (NO stretching), 1300−1162 cm^{-1} (NO_2 asymmetric stretching), and 1030−963 cm^{-1} (NO_2 symmetric stretching) in chelating and bridging bidentate transition metal complexes (*64*−*66*, *69*, *70*, *74*). In contrast, the NO stretching modes of ionic NO_3^- have appeared at 1440−1310 cm^{-1} (asymmetric NO stretching) and at 1068−1055 cm^{-1} (symmetric NO stretching) despite very weak IR intensity (*67*, *68*, *71*−*74*). The observed isotopic bands in the $^{14}NO_3^-/^{15}NO_3^-$ difference spectrum, shown in Figure 7, were present over the frequency range of 1400−1300 cm^{-1}, indicating that the $^{14}NO_3^-$ responsible for the isotopic bands in the difference spectrum exists over the frequency range of 1400−1370 cm^{-1}. Therefore, it is evident that the NO_3^- is not a metal binding form but an ionic form as illustrated in Figure 8A. This strongly indicates that NO_3^- is not associated with the Mn cluster as a direct ligand but is associated, in an ionic state, with a protein moiety of the Cl^- site. When the functional replacement of Cl^- with NO_3^- is taken into account, this suggests that Cl^- is not associated with the Mn cluster as a direct ligand. This view may be compatible with the reported results which show that the Mn K-edge XANES spectrum in Cl^--depleted membranes (*76*) and the deduced Mn−Mn distances in F^-- or Br^--substituted membranes (*31*, *33*) rather resemble those in the control membranes. No direct association of Cl^- with the Mn cluster is also consistent with the finding that I^--substituted membranes exhibit high O_2 evolving activity and TL bands arising from the S_2 and S_3 states (ref *26* and this study). If I^- is bound to the Mn cluster directly, I^- would readily reduce the Mn cluster in higher S states, interfering with the formation of the TL bands and the manifestation of the high O_2 rate. The Cl^- site must exist close to the Mn cluster but may be structurally separated from the cluster. Therefore, it is likely that Cl^- regulates the function of the OEC, including the Mn cluster, by optimizing the structure of protein matrixes of the OEC for water oxidation chemistry. Cl^--dependent activity control through conformation changes of protein that are induced by the binding of Cl^- to the allosteric site has been reported in *O*-acetylserine sulfhydrylase (*77*). It has been suggested that there are two types of Cl^- sites with differing affinities for Cl^- (*7*) and/or nature of the Cl^--depleted and anion-substituted OEC (*7*, *27*, *34*, *57*). We cannot, therefore, completely exclude the possibility that a small isotopic band from another NO_3^-, bound to the other type of Cl^- site, was induced but not detected in the difference spectrum due to the relatively low signal to noise ratio in the regions below 1200 cm^{-1} and above 1500 cm^{-1}.

Since the isotopic bands of NO_3^- correspond to the NO stretching mode for ionic NO_3^-, it can be presumed that bulk NO_3^-, or nonspecifically bound NO_3^- with a bulk-like nature, is responsible for the observed isotopic bands, apart from the mechanism of how such NO_3^- responds to oxidation of the Mn cluster. However, bulk NO_3^- reveals a significantly broadened NO stretching band with an approximate bandwidth of ∼100 cm^{-1} because of the presence of numerous combinations of bond lengths and bond angles among the three NO bonds (*75*) as shown in Figure 8B. It seems, then, that the bulk-like NO_3^- cannot account for the observed isotopic bands. The NO stretching band of NO_3^-, however, sharpens in salt crystals (*68*, *75*), which is compatible with the observed isotopic bands, suggesting that NO_3^- in a unique binding site is responsible for the isotopic bands. This seems to be compatible with the view that NO_3^- bound to the Cl^- site is responsible for the observed isotopic bands.

Model for the Isotopic Bands. In an ionic NO_3^- with D_{3h} symmetry, the NO asymmetric stretching vibrations are degenerate. However, the degeneracy is broken by a decrease in the geometrical symmetry of NO_3^-, resulting in the appearance of two split components with reduced intensity, in which the splitting depends on the difference between the three NO bond lengths, 16−93 cm^{-1} (*67*, *68*, *71*, *72*, *75*). The split-type bands have often been observed in the spectra of salt crystals (*68*, *71*, *72*, *75*). Taking this into account, and the fact that replacement of ^{14}N with ^{15}N leads to a downshift in the respective NO stretching mode of NO_3^- by 31−32 cm^{-1} (refs *67* and *71* and Figure 8B), we propose a simple model for interpreting the $^{14}NO_3^-/^{15}NO_3^-$ isotopic bands shown in Figure 9. For model IR bands, we used a Gaussian curve with a half-width at half-maximum of 16 and 31 cm^{-1} of the isotope downshift for $^{14}NO_3^-/^{15}NO_3^-$ (*67*, *71*). The $^{14}NO_3^-$ ($S_2Q_A^-/S_1Q_A$)/$^{15}NO_3^-$ ($S_2Q_A^-/S_1Q_A$) spectrum was used for fitting instead of the $^{14}NO_3^-$ (S_2/S_1)/$^{15}NO_3^-$ (S_2/S_1) spectrum due to the higher spectrum quality. In the observed $^{14}NO_3^-/^{15}NO_3^-$ difference spectrum, the intense positive (1369 cm^{-1}) and negative (1323 cm^{-1}) bands are mainly ascribed to the NO asymmetric stretching mode of $^{14}NO_3^-$ and $^{15}NO_3^-$ in the S_2 state, in which NO_3^- has symmetric geometry. While the minor negative (1406 cm^{-1}) and positive (1288 cm^{-1}) bands are ascribed to one of the split NO asymmetric stretching modes of $^{14}NO_3^-$ and $^{15}NO_3^-$ present in the S_1 state, in which NO_3^- has a rather asymmetric geometry. The intensity of the split bands can be assumed to be 50% of the degenerate band, although the intensity may be slightly altered depending on the geometry of NO_3^- (*75*). One of the NO stretching modes of $^{15}NO_3^-$ at 1372(−) cm^{-1} in the S_1 state contributes to the intensification of the 1369(+) cm^{-1} band of the observed $^{14}NO_3^-/^{15}NO_3^-$ difference spectrum, and one of the NO stretching modes of $^{14}NO_3^-$ at 1317(−) cm^{-1} in the S_1 state contributes to the

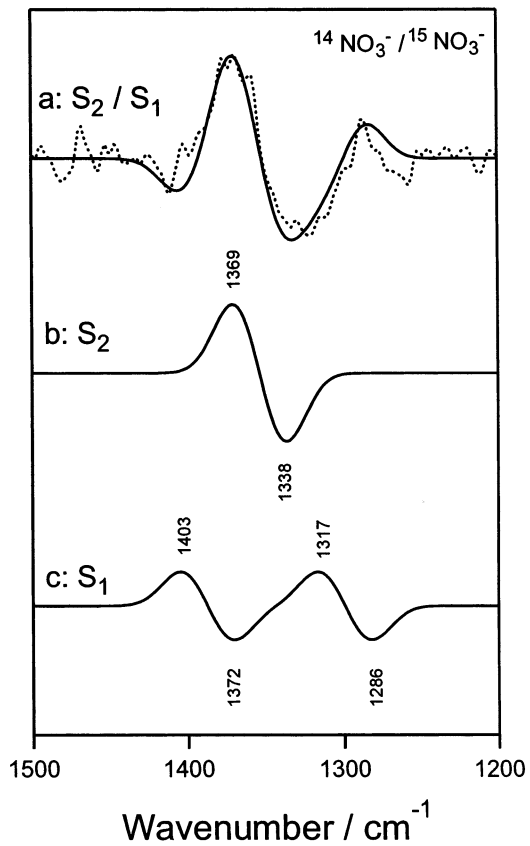

FIGURE 9: Simple model for the $^{14}NO_3^-/^{15}NO_3^-$ FTIR difference spectrum for the $S_2Q_A^-/S_1Q_A$ difference in Figure 7b. (a) The modeled $^{14}NO_3^-/^{15}NO_3^-$ spectrum for $S_2Q_A^-/S_1Q_A$ (—) compared with the experimental spectrum (···), (b) the modeled $^{14}NO_3^-/^{15}NO_3^-$ spectrum in the S_2 state, and (c) the modeled $^{14}NO_3^-/^{15}NO_3^-$ spectrum in the S_1 state. The Gaussian line shape was used for model IR bands. The modeled spectrum (a) was calculated by subtracting spectrum c from spectrum b. The $^{14}NO_3^-/^{15}NO_3^-$ spectrum for the $S_2Q_A^-/S_1Q_A$ difference is identical to that for the S_2/S_1 difference but has a better signal to noise ratio due to there being no $^{14}NO_3^-/^{15}NO_3^-$ isotopic effects on the Q_A^-/Q_A spectrum as shown in Figure 7c.

broadening of the 1323(−) cm^{-1} band of the observed spectrum.

According to this model, the bond lengths and bond angles of the three NO bonds are almost identical (highly symmetric) in the S_2 state, while the bond(s) of one (or two) NO group(s) is longer than the other two (or one) bonds (weakly asymmetric) in the S_1 state. A possible interpretation for the putative geometry change of NO_3^- is that the interaction between each oxygen atom and its ligand(s), protein or water molecule, is weak and equivalent in the S_2 state, while the stronger oxygen−ligand(s) interaction for two (or one) oxygen atoms gives the longer NO bond length in the S_1 state. These considerations may lead us to the view that NO_3^-, and thereby Cl^-, is bound to the site more strongly in the S_1 state than in the S_2 state. Significantly, it has been shown that the Cl^- affinity of the binding site is lower in the S_2 state than in the S_1 state (*22*), and that the replacement of Cl^- with NO_3^- is stimulated upon formation of the S_2 state (*13*). The higher Cl^- affinity in the S_1 state may be correlated with the stronger binding of Cl^- to the site in the S_1 state. Also, the nature of a binding site that prefers symmetric and weak binding in the S_2 state facilitates anion exchange at the site.

In general, vibrational NO stretching modes of NO_3^- depend on the NO force constant, which is mainly determined by the bond length of NO but is not directly correlated with the bond angle of NO_2 and the dihedral angle of the N−O bond with respect to the NO_2 plane. Therefore, our model does not distinguish the planar from the nonplanar geometry of NO_3^-. We note in this context, however, that the NO_3^- in all of the reported nitrato complexes is planar or planar-like as far as we know. Therefore, it is most likely that the NO_3^- bound to the Cl^- site in the OEC is also planar or planar-like. This view is also consistent with the easy replacement of Cl^- with NO_3^- in the medium, especially in the higher S states (*13*). However, we cannot completely exclude the possibility that the NO_3^- in the OEC is somehow distorted from the planar state by interacting with protein, although such a state may be thermodynamically unstable.

The observed $^{14}NO_3^-/^{15}NO_3^-$ difference spectrum may also be reproduced to some extent by a model in which the S_1 state has only one NO stretching band at 1317 cm^{-1} for $^{14}NO_3^-$ and at 1286 cm^{-1} for $^{15}NO_3^-$ with much reduced (30−40%) intensity. This model may be explained by assuming a degenerated NO asymmetric stretching band of NO_3^- with a symmetric geometry in the S_1 state. In this case, interactions between NO_3^- and its ligands are stronger on the whole to show the band at a lower frequency in the S_1 than in the S_2 state. However, we cannot rationally explain why the band intensity markedly decreases in the S_1 state compared with that in the S_2 state despite the same symmetric geometry of NO_3^- in both states. Alternatively, the appearance of one NO stretching band with a much reduced intensity in the S_1 state may be explicated by assuming an HNO_3-type molecule in the Cl^- binding site. HNO_3 exhibits NO stretching bands at ∼1320 cm^{-1} with strong intensity and at ∼1720 cm^{-1} with very weak intensity (*69*) in which the intensity of the 1320 cm^{-1} band is expected to be approximately 50% of that of the degenerated NO stretching of NO_3^-. However, it is hard to imagine that NO_3^- is bound to the Cl^- site as HNO_3 because of the observed high exchangeability of the bound NO_3^- with bulk NO_3^- ion. According to our unpublished ab initio MO calculation, NO stretching modes of NO_3^- could resemble those of HNO_3 if strong interaction with a positively charged imidazolium is assumed. A $^{14}NO_3^-$ $(S_2/S_1)/^{15}NO_3^-$ (S_2/S_1) difference spectrum with improved quality is needed to exclude these alternatives completely.

Effects of Cl^- Depletion and Anion Substitution. As shown in Figure 4, the Cl^- depletion induced characteristic changes in the symmetric carboxylate modes. Interestingly, the symmetric carboxylate modes that disappeared with Cl^- depletion are quite similar to those observed in the Ca^{2+}-depleted spectrum supplemented with Li^+, Na^+, and Mg^{2+}, cations having ionic radii that are smaller than that of Ca^{2+} (*78*). A possible interpretation of the characteristic S_2/S_1 carboxylate bands is that they are contributed by the two different carboxylates, which correspond to two different carboxylate ligands to the Mn cluster. One carboxylate ligand has a spectrum represented as that in the double-difference spectrum in Figure 4 and requires Cl^- for its conformation change upon the S_1 to S_2 transition. The other carboxylate ligand has a spectrum represented as that in the Cl^--depleted spectrum in Figure 4 and seems to be related to Ca^{2+}. Another interesting point we should emphasize is that the

features of the symmetric carboxylate mode found in the double-difference spectrum are surprisingly similar to those of the reported S_3/S_2 difference spectrum (*43*, *47*, *48*, *51*), although the positions of the respective bands are not identical to each other. Therefore, it may be deduced that the carboxylate ligand responsible for the S_3/S_2 spectrum is associated with the Mn cluster in a manner similar to that of the putative Cl^--sensitive carboxylate for the S_2/S_1 spectrum.

A characteristic spectral feature of the Cl^--depleted spectrum was the simplification of 1700−1500 cm^{-1} regions due to the absence of a large portion of the amide I and II bands. This indicates that Cl^- is required for the structural change of the protein backbone with the S_1 to S_2 transition, and the suppression of the structural change is ascribed to the inhibition of the normal turnover of the S state beyond the Cl^--depleted S_2 state. This is in contrast to the effects of Ca^{2+} depletion on the spectrum, where the amide bands are not much influenced by the depletion (*50*). Therefore, the results presented here clearly demonstrate that the functions of Ca^{2+} and Cl^- are quite different in regulating the protein structure in the vicinity of the S_2 state Mn cluster, although the S state turnover beyond the S_2 state is similarly interrupted in the absence of Ca^{2+} or Cl^-. The amide bands at 1674(−), 1668(+), 1660(−), 1637(−), and 1630(+) cm^{-1} were restored by Cl^- reconstitution, but these bands were barely recovered by anion substitution with Br^-, I^-, or NO_3^-, as shown in Figure 5. Since considerable O_2 evolution activity can be supported by these anions, the putative structure changes responsible for these bands are not essential for the mechanism of O_2 evolution. However, the changes may influence the redox and magnetic properties of the Mn cluster as revealed by the anion-dependent change of the $S_2Q_A^-$ TL band (Table l and refs *11*, *24*, and *26*) and the S_2 EPR signals (*2*, *34*), probably due to the close location of the Cl^- site to the cluster. These changes may be attributable to the slower turnover rate of the O_2 evolution found in the Br^--, I^--, or NO_3^--substituted OEC (Figure 1). In contrast to Br^-, I^-, and NO_3^-, both amide and carboxylate bands were markedly suppressed in F^-- or CH_3COO^--substituted membranes. Since the S_2 state can be generated in the substituted membranes, as indicated by the formation of the $S_2Q_A^-$ TL band (refs *11* and *24* and Table 1) and/or S_2 EPR signal (*24*, *29*, *32*, *33*), it appears that the binding of F^- or CH_3COO^- induces further structural perturbations to interrupt the formation of the FTIR bands. The deteriorating protein structure may be ascribed to the fact that these anions have no or a poor ability to support a high O_2 evolution rate. The results indicate that not only a negative charge but also some physical property of the anion is important for its function in the OEC.

REFERENCES

1. Debus, R. J. (1992) *Biochim. Biophys. Acta 1102*, 269−352.
2. Britt, R. D. (1996) in *Oxygenic Photosynthesis: The Light Reactions* (Ort, D. R., and Yocum, C. F., Eds.) pp 137−164, Kluwer Academic Publishers, Dordrecht, The Netherlands.
3. Renger, G. (2001) *Biochim. Biophys. Acta 1503*, 210−228.
4. Crichley, C. (1985) *Biochim. Biophys. Acta 811*, 33−46.
5. Homann, P. H. (1987) *J. Bioenerg. Biomembr. 19*, 105−123.
6. Lindberg, K., Wydrzynski, T., Vänngård, T., and Andréasson, L.-E. (1990) *FEBS Lett. 264*, 153−155.
7. Lindberg, K., and Andréasson, L.-E. (1996) *Biochemistry 35*, 14259−14267.
8. Akabori, K., Imaoka, A., and Toyoshima, Y. (1984) *FEBS Lett. 173*, 36−40.
9. Miyao, M., and Murata, K. (1985) *FEBS Lett. 180*, 303−307.
10. Homann, P. H. (1988) *Photosynth. Res. 15*, 205−220.
11. Homann, P. H. (1993) *Photosynth. Res. 38*, 395−400.
12. Lindberg, K., Vängård, T., and Andréasson, L.-E. (1993) *Photosynth. Res. 38*, 401−408.
13. Wincencjusz, H., Yocum, C. F., and van Gorkom, H. J. (1998) *Biochemistry 37*, 8595−8604.
14. Preston, C., and Pace, R. J. (1985) *Biochim. Biophys. Acta 810*, 388−391.
15. Itoh, S., Yerkes, C. T., Koike, H., Robimson, H. H., and Crofts, A. R. (1984) *Biochim. Biophys. Acta 766*, 612−622.
16. Theg, S. M., Jursinic, P. A., and Homann, P. H. (1984) *Biochim. Biophys. Acta 766*, 636−646.
17. Homann, P. H., Gleiter, H., Ono, T.-a., and Inoue, Y. (1986) *Biochim. Biophys. Acta 850*, 10−20.
18. Ono, T., Zimmermann, J. L., Inoue, Y., and Rutherford, A. W. (1986) *Biochim. Biophys. Acta 851*, 193−201.
19. Ono, T.-a., Noguchi, T., Inoue, Y., Kusunoki, M., Yamaguchi, H., and Oyanagi, H. (1995) *J. Am. Chem. Soc. 117*, 6386−6387.
20. Baumgarten, M., Philo, J. S., and Dismukes, G. C. (1990) *Biochemistry 29*, 10814−10822.
21. Boussac, A., Sétif, P., and Rutherford, A. W. (1992) *Biochemistry 31*, 1224−1234.
22. Wincencjusz, H., van Gorkom, H. J., and Yocum, C. F. (1997) *Biochemistry 36*, 3663−3670.
23. Sandusky, P. O., and Yocum, C. F. (1984) *Biochim. Biophys. Acta 766*, 603−611.
24. Ono, T.-a., Nakayama, H., Gleiter, H., Inoue, Y., and Kawamori, A. (1987) *Arch. Biochem. Biophys. 256*, 618−624.
25. Wincencjusz, H., Yocum, C. F., and van Gorkom, H. J. (1999) *Biochemistry 38*, 3719−3725.
26. Rashid, A., and Homann, P. H. (1992) *Biochim. Biophys. Acta 1101*, 303−310.
27. van Vliet, P., and Rutherford, A. W. (1996) *Biochemistry 35*, 1829−1839.
28. Haddy, A., Hatchell, J. A., Kimel, R. A., and Thomas, R. (1999) *Biochemistry 38*, 6104−6110.
29. Casey, J. L., and Sauer, K. (1984) *Biochim. Biophys. Acta 767*, 21−28.
30. Krieger, A., Rutherford, A. W., and Jegerschöld, C. (1998) *Biochim. Biophys. Acta 1364*, 46−54.
31. Klein, M. P., Sauer, K., and Yachandra, V. K. (1993) *Photosynth. Res. 38*, 265−277.
32. Force, D. A., Randall, D. W., and Britt, R. D. (1997) *Biochemistry 36*, 12062−12070.
33. DeRose, V. J., Latimer, M. J., Zimmermann, J.-L., Mukerji, I., Yachandra, V. K., Sauer, K., and Klein, M. P. (1995) *Chem. Phys. 194*, 443−459.
34. Boussac, A. (1995) *Chem. Phys. 194*, 409−418.
35. Noguchi, T., Ono, T., and Inoue, Y. (1992) *Biochemistry 31*, 5953−5956.
36. Noguchi, T., Ono, T., and Inoue, Y. (1993) *Biochim. Biophys. Acta 1143*, 333−356.
37. Noguchi, T., Ono, T., and Inoue, Y. (1995) *Biochim. Biophys. Acta 1228*, 189−200.
38. Noguchi, T., Ono, T., and Inoue, Y. (1995) *Biochim. Biophys. Acta 1232*, 59−66.
39. Noguchi, T., Inoue, Y., and Tang, X.-S. (1997) *Biochemistry 36*, 14705−14711.
40. Noguchi, T., Inoue, Y., and Tang, X.-S. (1999) *Biochemistry 38*, 10187−10195.
41. Chu, H.-A., Gardner, M. T., O'Brien, J. P., and Babcock, G. T. (1999) *Biochemistry 38*, 4533−4541.
42. Noguchi, T., and Sugiura, M. (2000) *Biochemistry 39*, 10943−10949.
43. Chu, H.-A., Sacett, H., and Babcock, G. T. (2000) *Biochim. Biophys. Acta 1459*, 528−532.
44. Onoda, K., Mino, H., Inoue, Y., and Noguchi, T. (2000) *Photosynth. Res. 63*, 47−57.
45. Chu, H.-A., Gardner, M. T., Hillier, W., and Babcock, G. T. (2000) *Photosynth. Res. 66*, 57−63.
46. Chu, H.-A., Hillier, W., Law, N. A., and Babcock, G. T. (2001) *Biochim. Biophys. Acta 1503*, 69−82.
47. Noguchi, T., and Sugiura, M. (2001) *Biochemistry 40*, 1497−1502.
48. Hillier, W., and Babcock, G. T. (2001) *Biochemistry 40*, 1503−1509.

49. Chu, H.-A., Debus, R. J., and Babcock, G. T. (2001) *Biochemistry 40*, 2312−2316.
50. Kimura, Y., and Ono, T.-a. (2001) *Biochemistry 40*, 14061−14068.
51. Noguchi, T., and Sugiura, M. (2002) *Biochemistry 41*, 2322−2330.
52. Noguchi, T., Ono, T., and Inoue, Y. (1995) in *Photosynthesis: from Light to Biosphere* (Mathis, P., Ed.) Vol. II, pp 235−240, Kluwer Academic Publishers, Dordrecht, The Netherlands.
53. Berthold, D. A., Babcock, G. T., and Yocum, C. F. (1981) *FEBS Lett. 134*, 231−234.
54. Ono, T.-a., and Inoue, Y. (1986) *Biochim. Biophys. Acta 850*, 380−389.
55. Izawa, S., and Ort, D. R. (1974) *Biochim. Biophys. Acta 357*, 127−143.
56. Homann, P. H. (1985) *Biochim. Biophys. Acta 809*, 311−319.
57. Damoder, R., Klimov, V. V., and Dismukes, G. C. (1986) *Biochim. Biophys. Acta 848*, 378−391.
58. Hienerwadel, R., Boussac, A., Breton, J., and Berthomieu, C. (1996) *Biochemistry 35*, 15447−15460.
59. Zhang, H., Razeghifard, M. R., Fischer, G., and Wydrzynski, T. (1997) *Biochemistry 36*, 11762−11768.
60. Razeghifard, M. R., Kim, S., Patzlaff, J. S., Hutchison, R. S., Krick, T., Ayala, I., Steenhuis, J. J., Boesch, S. E., Wheeler, R. A., and Barry, B. A. (1999) *J. Phys. Chem. B 103*, 9790−9800.
61. Ayala, I., Kim, S., and Barry, B. A. (1999) *Biophys. J. 77*, 2137−2144.
62. Kim, S., Patzlaff, J. S., Krick, T., Ayala, I., Sachs, R. K., and Barry, B. A. (2000) *J. Phys. Chem. B 104*, 9720−9727.
63. Noguchi, T., Sugiura, M., and Inoue, Y. (1999) in *Fourier Transform Spectroscopy* (Itoh, K., and Tasumi, M., Eds.) pp 459−460, Waseda University Press, Tokyo.
64. Gatehouse, B. M., Livingstone, S. E., and Nyholm, R. S. (1958) *J. Inorg. Nucl. Chem. 8*, 75−78.
65. Addison, C. C., and Simpson, W. B. (1965) *J. Chem. Soc.*, 598−602.
66. Addison, C. C., Amos, D. W., and Sutton, D. (1967) *J. Chem. Soc. A*, 808−812.
67. Kato, R., and Rolfe, J. (1967) *J. Chem. Phys. 47*, 1901−1910.
68. James, D. W., and Leong, W. H. (1968) *J. Chem. Phys. 56*, 5089−5096.
69. Addison, C. C., Logan, N., and Wallwork, S. C. (1971) *Q. Rev. (London) 25*, 289−322.
70. Johnson, D. W., and Sutton, D. (1972) *Can. J. Chem. 50*, 3326−3331.
71. von Becher, H. J., Friedrich, F., and Willner, H. (1976) *Z. Anorg. Allg. Chem. 426*, 15−27.
72. Yamamoto, A., Utida, T., Murata, H., and Shiro, Y. (1976) *J. Phys. Chem. Solids 37*, 693−698.
73. Belousov, M. V., Pogarev, D. E., and Shultin, A. A. (1978) *Sov. Phys. Solid State 20*, 814−816.
74. Nakamoto, K. (1997) *Infrared and Raman Spectra of Inorganic and Coordination Compounds: Part A and B*, 5th ed., Wiley, New York.
75. Waterland, M. R., Stockwell, D., and Kelley, A. M. (2001) *J. Chem. Phys. 114*, 6249−6258.
76. Ono, T.-a., Noguchi, T., Inoue, Y., Kusunoki, M., Yamaguchi, H., and Oyanagi, H. (1995) *Photon Factory Activity Rep. 12*, 57.
77. Burkhard, P., Tai, C.-H., Jansonius, J. N., and Cook, P. F. (2000) *J. Mol. Biol. 303*, 279−286.
78. Kimura, Y., Hasegawa, K., and Ono, T. (2002) *Biochemistry 41*, 5844−5853.

BI026595N